Journal of Energy Storage 54 (2022) 105260

Contents lists available at ScienceDirect

Journal of Energy Storage

journal homepage: www.elsevier.com/locate/est

Research papers

In-situ temperature monitoring of a lithium-ion battery using an embedded thermocouple for smart battery applications

B. Gulsoy *, T.A. Vincent, J.E.H. Sansom, J. Marco

WMG, University of Warwick, Coventry CV4 7AL, United Kingdom

ARTICLE INFO

Keywords:
Lithium-ion battery
Cell instrumentation
Embedded sensing
In-situ monitoring
Internal temperature
Cell performance
Battery ageing

ABSTRACT

Uncertainty in the measurement of key battery internal states, such as temperature, impacts our understanding of battery performance, degradation and safety and underpins considerable complexity and cost when scaling-up battery components into complete systems. Our research presents a systematic methodology for the engineering of a commercially available cylindrical cell format to accept in-cell instrumentation. We have developed bespoke cell opening methods and unique fixtures that facilitate a reliable instrumentation process. Extensive experimental results are presented that highlight the performance of both the sensor and the lithium-ion battery are not adversely affected by instrumentation. Our modified test cells were evaluated the energy capacity and impedance for a range of different electrical loading conditions and compared to a set of reference or unmodified batteries. The longer-term implications of embedding instrumentation within a battery are also evaluated with cell performance evaluated after a period of calendar and cyclic ageing. Our study demonstrates the importance of internal temperature monitoring during cell operation by comparing internal and surface temperatures measurements. We found that the internal temperature is consistently and notably higher than surface temperature during cell characterisation and when the cell was electrically loaded with a dynamic real-world profile derived from an electric vehicle. No significant effect on the electrochemical performance of the instrumented cells was observed. Measurement data demonstrates that there is a negligible reduction in energy capacity and only a marginal increase in internal resistance.

1. Introduction

Many countries have publicly committed to decarbonise their transport systems between the years 2030–2050 [1]. This requirement mandates the electrification of multiple sectors and the use of battery technology to replace traditional fossil fuels. A complete battery system will often consist of many hundreds of lithium-ion batteries (LIBs) combined electrically. Cell-to-cell manufacturing variations, combined with the impact factors including interconnection resistance and temperature differences between cells makes the management and monitoring of key battery states, such as state of charge (SOC) and state of health (SOH) a highly challenging task and one where there is no universally accepted solution [2,3]. Currently, many battery parameters are estimated through a combination of mathematical modelling and data collection using traditional surface-mount sensor technology (e.g., temperature, voltage and current). The challenges with this approach are three-fold. Firstly, the mathematical model employed is tightly coupled to the physical format and electrochemistry of the battery. Secondly, the fidelity of the model is often limited and will not represent many physical phenomena. Finally, the accuracy and robustness of battery state estimation is known to reduce as the battery ages and its electrochemical properties change. Lack of understanding of cell internal processes and the inability to measure internal parameters underpins considerable complexity and cost when scaling-up battery components into complete systems, e.g., for electric vehicles (EVs). The uncertainty of measuring SOC directly impacts the estimation of driving range and the ability to fast-charge the vehicle. The problem is more acute for future all-electric aircraft. Regulatory bodies mandate that redundancy must be included, in the form of additional battery capacity, to ensure safe aircraft operation.

Abbreviations: EV, electric vehicles; LIB, lithium-ion batteries; OCV, open circuit voltage; SOH, state of health; Z, internal impedance; FBG, Fibre Bragg Grating; CT, x-ray computed tomography; KN, alumel; KP/EP, chromel; RPT, reference performance test; DC, direct current; DCIR, direct current internal resistance; CC, constant current; CV, constant voltage.

* Corresponding author.
E-mail address: begum.gulsoy.1@warwick.ac.uk (B. Gulsoy).

https://doi.org/10.1016/j.est.2022.105260
Received 18 March 2022; Received in revised form 23 May 2022; Accepted 1 July 2022

There is a great interest in the field of battery sensing and SOH evaluation. Research is often focussed on new methods of battery management or characterisation techniques to underpin our understanding of LIB degradation or safety. Our research is focussed on transforming the LIB from a passive component into a mechatronic device, through the integration of sensing, communication, and controller hardware directly within the battery. The research presented here addresses the need to quantify internal cell temperature and the differential between internal and external cell temperatures during LIB operation at the onset of battery life and after the battery management has been subject to both calendar and cyclic ageing. The systematic methodology employed to engineer the cells to accept the new temperature sensor without adversely affecting energy capacity, internal resistance and expected life are described in detail within this report.

The close coupling between thermal management and LIB performance, degradation and safety has been the subject of considerable research. For example, the presence of radial temperature gradients inside a cylindrical cell have been studied by Zhang et al. [4], through the placement of micro thermocouples within the jelly-roll. In their study, the thermocouple tips were designed to be approximately 80 μm in diameter, with a Parylene protective layer to prevent chemical damage inside the cell. Smaller diameter thermocouples were available, but their use was avoided due to their physical fragility. In the study by Zhang et al. [5], was noted that poor thermal conductivity through the electrodes and separator within the cross-plane direction (circa:1 W $(mK)^{-1}$) leads to high discrepancies between surface and internal temperatures. During a 3C discharge, the internal temperature was found to almost 5 °C higher than its reference surface thermocouple. Compared to an unmodified cell, a minimal difference in cell voltage was observed across a discharge cycle (within tolerances, <0.1 V). Although this demonstrates the initial success of this instrumented cell, Zhang et al. do not present results for testing the cell over a longer period of ageing. Further, this study does not include any comparative analysis of capacity or cell resistance variations that may arise due to in-cell instrumentation.

As an alternative to thermocouple sensing, fibre optic sensing methods have previously been suggested as a suitable method to measure the temperature within a LIB [6]. Typically, researchers use Fibre Bragg Grating (FBG) sensors, which are often favoured for their increasing commercial availability, comparatively low cost, chemical integrity to reaction with cell electrolyte and immunity to electromagnetic interference [7]. These distributed sensors offer improved spatial resolution (e.g. a 2.6 mm resolution sensor was used by Yu et al. [6]) to facilitate the distributed measurement of temperature over the surface or within a larger format cell. However, these sensor types require costly and physically large measurement equipment, prohibiting their deployment within battery systems or complete battery packs. The thin diameter of fibres, typically up to 200 μm [8] including cladding, means they require only minimal disruption to the cell structure, although their fragile nature usually mandates the use of additional sheathing. Diameters of up to 1.6 mm have been reported in recent studies. However, it is noted that reducing this dimension is a key point of interest within this field of research [9]. Due to their fragility, delicate handling is required during instrumentation. This further hinders deployment in many end-use applications, where mechanical excitation such as vibration or shock may damage the sensor.

Pioneering research that employed fibre optic sensors demonstrated the need for careful core temperature monitoring during pack design. Temperature differential of up to 5 °C (between cell internals and surface) have been reported, when a cylindrical cell is charged at a modest rate of 2.2C [10]. When a similarly instrumented cell was charged and discharged at a rate of 1C, internal temperatures exceeded the surface temperatures by between 3 and 6 °C, respectively. This leads the authors to conclude that surface temperature measurements were not representative or sufficiently comprehensive to understand cell performance and to optimise battery system operation [11].

Table 1
Previous relevant articles studying internal cell temperature.

Sensor type	Cell type	Experiment notes/findings	Reference
Custom miniature thermocouple	21700 cylindrical	Robust instrumentation into centre of cell core. Demonstrating need for internal temperature measurement.	This work.
Custom miniature thermocouples	18650 cylindrical	Thermocouples radial distributed within jellyroll of cell to demonstrate poor heat conduction from cell core to surface.	Zhang et al. [4]
Thermistor array	21700 cylindrical	Distributed sensing (10 mm spatial resolution) along core of cell. Investigating gradients along length of cell.	Vincent et al. [17]
Thermistor array	Pouch and 18650 cylindrical cells	Embedded flexible distributed sensing along the cell length. Investigating in-situ and operando thermal behaviour.	Fleming et al. [18]
Thermistor sensor	21700 cylindrical	Single resistive temperature sensor deployed in cell with wireless transmission system.	Yang et al. [19]
FBG sensor	A5 pouch	Distributed sensing (serpentine across internal area of pouch cell). Demonstrating hotter and cooler regions as cell cycled.	Yu et al. [6]
FBG sensor	18650 cylindrical	Proof-of-concept cell instrumentation. Demonstrating core temperature sensing, also combining reference electrode sensing.	McTurk et al. [9–11]
FBG sensor	Pouch (16 cm^2 area)	Placement of sensor inside pouch, demonstrating inhomogeneous heat distribution across cell active area.	Novais et al. [20]
Thermocouples	Pouch prismatic and 21700 cylindrical	Insertion of sensors inside pouch, prismatic and cylindrical cells demonstrating internal temperature detection of thermal runaway.	Xu et al. [16]
Hard and soft sensors	Pouch cylindrical and prismatic	Review the most recent studies of internal temperature monitoring by the comparison of hard (required to be inserted into the cell) and soft sensors (uses estimation methods).	Jinasena et al. [21]

Fleckenstein et al. reviewed the harsh ageing conditions where in a simulated cycle which included a 16C charge rate. Researchers noted a significant temperature differential of around 20 °C between the internal and external components of the cell at the end of the cycle [12]. Srinivasan et al. noted that abnormal ageing processes can occur due to inadequate cooling and material/cell manufacturing tolerances [13]. Chombo et al. also highlighted that faster ageing can eventuate due to non-uniform cooling [14]. Richardson et al. highlighted in order to prevent these defects from leading to failure or excessive degradation at the system scale, internal temperature monitoring is critical to identify abnormal heat generation [15].

During thermal runaway experiments, Xu et al. found a significantly greater temperature rise was experienced internally when compared to that measured on the cell surface. At the peak of thermal runaway, the internal temperature of the cylindrical cell exceeded 1220 °C (compared to a surface temperature of only 600 °C), demonstrating the importance

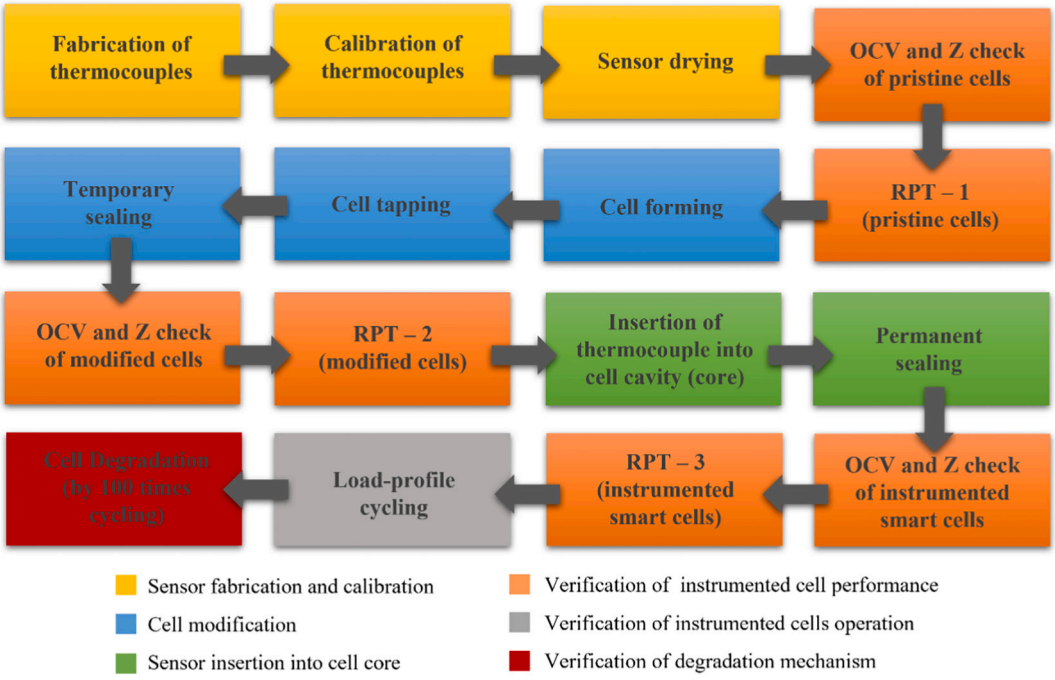

Fig. 1. Cell instrumentation stages including verification tests performed in this work.

of measuring internal temperature, when investigating the onset of thermal runaway [16]. Previous works on cell instrumentation that include the experimental in-cell measurement of temperature are included in Table 1. The summary highlights pertinent information such as: cell format, sensor type and the experimental objective of the research.

For the work reported here we have chosen to use bespoke ceramic K-type thermocouple sensors for measuring internal cell temperature conditions. Thermocouples are simple and robust sensors which can be contained within protective tubing and can be deployed into a range of harsh cell environments. The subject of sensor deployment was reviewed in detail by Jinasena et al. [21], where it was noted thermocouples have proven to be reliable in and around commercial battery packs. Thermocouples, e.g., K-type, are typically inexpensive to produce. High performance thermocouples with a measurement resolution in the order of 0.03 °C and can cover wide operating range (up to 1200 °C) [22]. K-types are already mass produced and their contraction and materials can be tailored to the application. Their temperature dependent analogue output voltage can also be easily integrated with precision laboratory measurement device and battery management control hardware [23].

For in-cell instrumentation, entry to the cell via the negative terminal is often preferred to minimise disruption to the internal components and the cell safety mechanism. This mechanism includes pressure release cap and PTC (if fitted) [24]. There have been previous reports of drilling into the aluminium can of cylindrical cells. For example in Xu et al. [16] have reported drilling into the can of cylindrical cell. However, limited information is detailed regarding the methodology, and in particular, the steps taken to ensure that metal fragments or swarf do not enter the cell. Such an occurrence would represent a safety concern, since metal fragments could result in an internal short-circuit. The research also fails to provide experimental results that demonstrate the long-term performance of the instrumented cells.

A drilling technique involving a 'plug cutter' drill bit was developed by Belt et al. [25]. The possible short circuit risk with metal shards was identified by the authors. To counteract this issue a bespoke drill bit was constructed with a hollow centre, thereby reducing the risk of metal debris entering the cell. They used the method to instrument their cells with reference electrodes to measure individual electrode potentials. The study incorporated a procedure to monitor cell degradation, e.g., capacity fade and resistance rise. However, the authors acknowledged that a longer-term durability study was not evaluated in their work. Also, this initial research relied upon near-complete cell disassembly where the sensors were inserted into the cells and then secured into place using glue.

Our research extends these previous studies into methods of cell modification to accept internal instrumentation. We have developed bespoke cell opening methods and unique fixtures that underpin a reliable instrumentation process. Extensive experimental results are presented that highlight the performance of both the sensor and the cell are not adversely affected by the instrumentation process. Our modified test cells were evaluated the energy capacity and impedance for a range of different electrical loading conditions and compared to a set of reference or unmodified batteries. The longer-term implications of embedding instrumentation within a battery are also evaluated with cell performance evaluated after a period of calendar and cyclic ageing.

This paper is structure of the paper as follows. Cell instrumentation is discussed in Section 2.

Section 2 discusses, in detail, the cell modification, instrumentation and verification methodology adopted in this research. Results and discussion are presented in Section 3, with further work and conclusions provided in Section 4 and 5 respectively.

2. Experimental methodology

The process flow diagram in Fig. 1 illustrates the experimental stages employed for cell instrumentation including: sensor fabrication, cell modification and sensor insertion. The diagram highlights the different verification stages for assessing cell performance, operation and ageing.

2.1. Sensor fabrication and calibration

Thermocouple devices were selected as suitable sensor types for internal cell instrumentation. In our research, the developed thermocouples (*research thermocouples*) were fabricated using a twin bore ceramic tube (1.55 mm diameter and 150 mm length). Material selection was

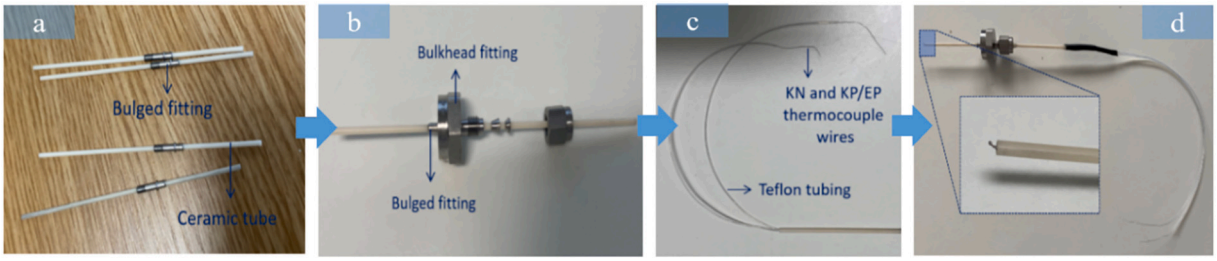

Fig. 2. Research thermocouple fabrication process. (a) Assembly of bulged fitting on a ceramic tube, (b) assembly of bulkhead and bulged fittings, (c) insertion of thermocouple wires into ceramic tube and covered with Teflon tubing, (d) welding of thermocouple wires.

Table 2
Calibration results from the three research thermocouples.

Thermocouples	Temperature (°C)							Accuracy (±°C)
Reference A	19.90	24.80	29.76	34.70	39.66	44.59	49.53	NA
Research thermocouple A	19.75	24.67	29.63	34.56	39.54	44.48	49.41	0.29
Reference B	18.99	24.05	29.12	34.21	39.29	44.36	49.44	NA
Research thermocouple B	18.81	23.88	28.95	34.09	39.20	44.28	49.38	0.32
Reference C	18.43	23.47	28.60	33.77	38.91	44.01	49.15	NA
Research thermocouple C	18.54	23.57	28.66	33.84	38.98	44.10	49.21	0.25

based on affordability, the availability of the material to support potential scale-up to volume production and the ability to measure a suitable temperature range (e.g. 20 to 750 °C). K-type thermocouples were used ensuring compatibility with industry standard measurement equipment and the integration of the sensor into existing battery test equipment. By constructing the thermocouples from first principles, we were able to customise their dimensions to suit the physical requirements of sensor insertion within the cell.

Custom fittings were designed and fabricated to facilitate a secure housing for the sensor within the cell. An image of the research thermocouple fabrication process is shown in Fig. 2. Stainless steel bulkhead fittings, (Swagelok SS-100-1-OR), were employed to maintain the mechanical resilience of the cylindrical cells. As shown in Fig. 2(a), to securely re-seal the cell after sensor insertion, the twin bore ceramic tube was assembled with a threaded bulged tube. The parallel thread of the bulkhead fitting was replaced with a bulged tube adapter as shown in Fig. 2(b). The fitting was designed to enable the location of the measuring tip within the cell cavity to be adjustable. This capability supports the instrumentation of different commercially available cell formats, such as 18650 or 21700. In this work, the bespoke fittings were assembled 35 mm (mid-way along axial length of the cell). This distance was selected to enable monitoring of temperature centrally within the cell core, where a significant thermal difference is expected when comparing against the measured surface temperature [9,10,26]. Chromel alumel (KN and KP/EP) thermocouple wires were inserted into the holes of the twin bore ceramic tube and covered with Teflon tubing as shown in Fig. 2(c). Finally, Fig. 2(d) shows the thermocouple wires welded using fine thermocouple welder (via RS PRO® fine thermocouple welder).

A total of three research thermocouples were fabricated. All research thermocouples were calibrated within the temperature range of 20 °C to 50 °C, which covers the range of nominal cell operation [27]. Calibration was performed in a climate chamber (Binder MKF56). For precise temperature calibration, a reference thermocouple (K-type, ±0.5 °C accuracy up to 50 °C) was fitted to each research thermocouple. The temperature within the climate chamber was increased in steps of 5 °C, at intervals of 120 min. Temperature measurements were made at a sample-rate of 10 Hz via a data logger (TC-08, Pico Technology, UK). The calibration results shown in Table 2 highlight that the research thermocouples (Thermocouple A, B and C) show a good correlation to the commercial reference device. The uncertainty from the measuring system was found to be ±0.143 °C and this is included in the accuracy estimation of each sensor. Prior to inserting within the target cell, the research thermocouples were dried within a vacuum oven for 6 h at 40 °C, to reduce humidity and to minimise the potential of introducing moisture into the cell during the assembly process.

2.2. Cell modification

Commercial cylindrical cells LG-M50 (21700 format) were selected for instrumentation. These cells are popular in automotive and energy storage applications, due to their energy density and relatively long

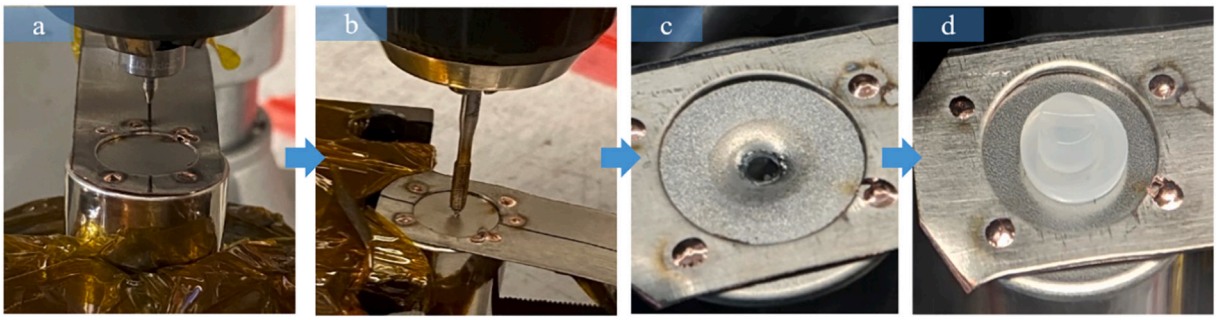

Fig. 3. Images of the cell modification process. (a) Forming a hole on the negative terminal of LG-M50 cell, (b) tapping the hole, (c) image of the hole on the negative terminal, (d) temporarily sealing for the primary verification and inspection.

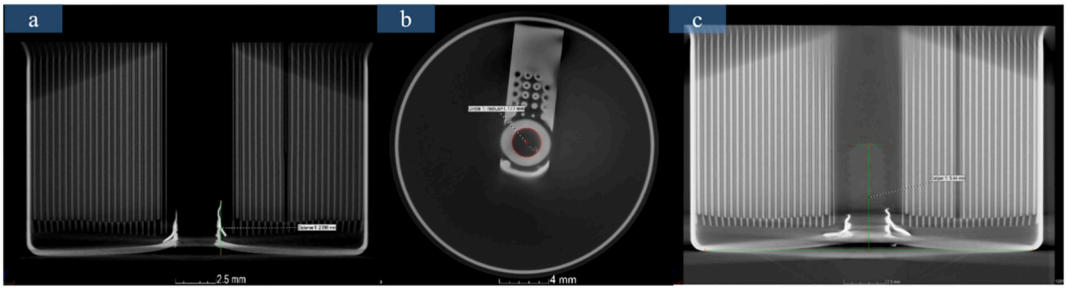

Fig. 4. X-ray computed tomography (CT) images of modified cell. (a) A side view of the negative terminal, (b) top view of negative terminal, (c) opening resealed with a Nylon screw.

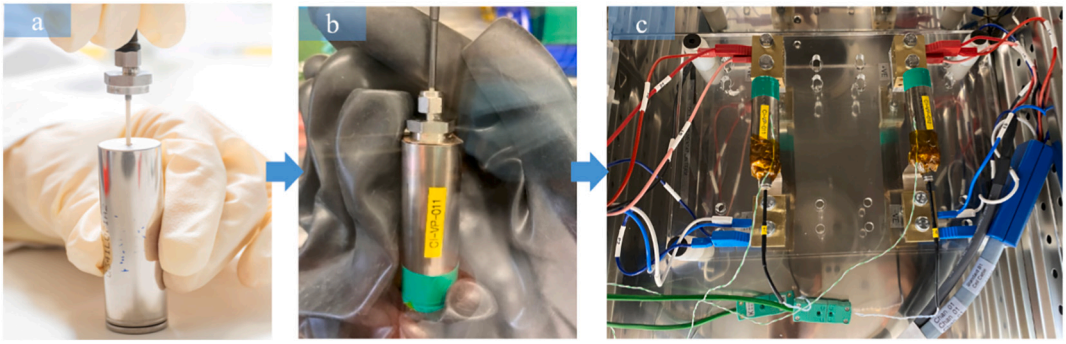

Fig. 5. Sensor insertion and instrumented cell testing. (a) Sensor alignment, (b) cell resealing, (c) instrumented cell testing.

cycle-life [28]. The cells comprise a NMC 811 formulation for the cathode and a Graphite-SiO_x anode. The manufacturer's datasheet defines an energy capacity of 5 Ah and an operational voltage range of 2.5 V to 4.2 V [29]. Prior to modification, each cylindrical cell was discharged to 3 V at a constant current rate of C/3 (process defined further in Section 3.4) using a Bio-Logic VSP-300 Potentiostat. The reduced SOC was selected to minimise potential safety hazards from short-circuits that may result from inadvertently damaging the jelly-roll caused by incorrect cell opening or sensor insertion. To support this study, three LG-M50 cells were instrumented.

The cell opening procedure was conducted within an argon-filled glove box, where $O_2$and H_2O concentrations were maintained below 0.1 ppm. The cell modification process is shown in Fig. 3. The first stage is to form a pilot hole located in the centre of the negative terminal, to guide a threading tap. This hole provides access directly into the hollow mandrel of the cylindrical cell (Ø 3 mm by CT scanning), forming a reliable instrumentation port without causing significant mechanical damage to the integrity of the cell case or its internal components. The pilot hole is formed using a flow-drill bit (with a diameter of 1.8 mm) via a bench pillar drill as shown in Fig. 3(a). A thread was formed using a custom tapping bit as shown in Fig. 3(b). The thread on the negative terminal, illustrated in Fig. 3(c) provides a reliable means to re-seal the instrumented cell after insertion of the sensor. The modified cylindrical cells were temporarily re-sealed with a nylon screw and washer assembly, illustrated in Fig. 3(d). This allows for the intermediate verification of the modified cell before instrumentation (see Section 3.4) and visual inspection of the cell while avoiding electrolyte leakage from the negative terminal.

X-ray computed tomography (CT) images of the cell recorded after each stage of the instrumentation process are shown in Fig. 4. The mechanical thread, the hole made in the can/internal tab and the use of the nylon screw to reseal the modified cell are clearly visible.

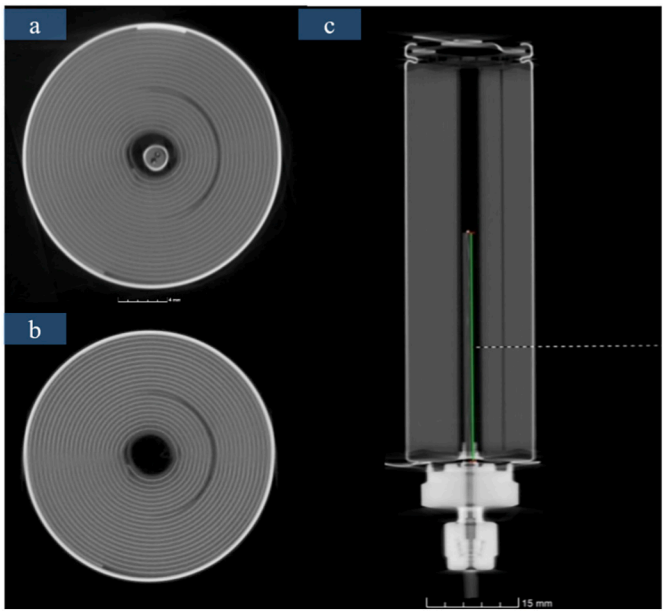

Fig. 6. X-ray computed tomography (CT) images of an instrumented cell. (a) The top view of the negative terminal after instrumentation: (b) the top view of the positive terminal, (c) the side view of the instrumented cell.

2.3. Sensor insertion into cell core

The insertion of the research thermocouples within each of the modified cells was performed inside an argon-filled glove box, where O_2 and H_2O concentrations were again maintained below 0.1 ppm. Fig. 5 illustrates the overall processes from sensor insertion through to cell testing in which its electrical properties are fully characterised. With the temporary seal removed, a research thermocouple was positioned

Table 3
Measured OCV and impedance values after each stage of cell modification process.

Cell No	Pristine		Modified				Instrumented			
	Voltage (V)	Impedance (mΩ)	Voltage (V)	D_V (%)	Impedance (mΩ)	D_Z (%)	Voltage (V)	D_V (%)	Impedance (mΩ)	D_Z (%)
Cell 1	3.16	23.19	3.16	0	23.58	1.68	3.13	0.95 (–)	23.84	2.80
Cell 2	3.16	23.35	3.15	0.32 (–)	23.86	2.18	3.12	1.27 (–)	24.14	3.38
Cell 3	3.17	23.37	3.16	0.32 (–)	23.74	1.58	3.12	1.58 (–)	23.98	2.61

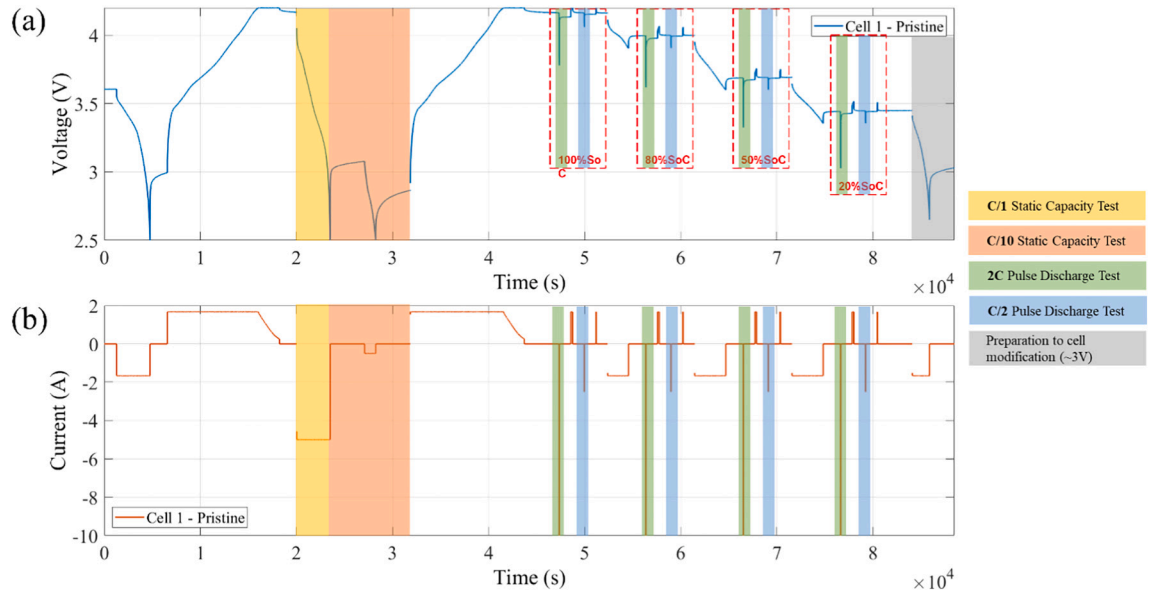

Fig. 7. Reference performance test (RPT) profile used in this research. (a) Cell voltage during the RPT with (LG-M50) cell 1 before cell modification (pristine condition), (b) current applied to the cell during the RPT.

perpendicular to the negative terminal as show in Fig. 5(a). The thermocouple was carefully inserted perpendicular into the cell cavity to avoid misalignment of the sensor hence minimising the risk of damage to the jelly-roll. The bulkhead fitting was employed to screw into the cell body to re-seal the cell. An example of one instrumented cell is shown in Fig. 5(b).

The CT images of the cell after sensor insertion are shown in Fig. 6. The images illustrate that there is no damage in the jelly-roll due to sensor insertion. The green highlighted area in Fig. 6(c) shows the positioning of the research thermocouple, exactly half-way along the axial length of the cell.

The open circuit voltage (OCV) and internal impedance (Z) of the modified and instrumented cells was measured using a battery tester (Hioki BT3564) before and after modification and sensor insertion. This initial test provides an efficient method to assess the success of the instrumentation process. A more detailed verification strategy is defined in Section 3.4. Table 3 summarises the OCV and impedance measurements for each experimental cell, including the measured variation compared to the unmodified or *pristine* cell. D_V(%) and D_Z (%) define the voltage and impedance change respectively. Comparing values before and after each cell was modified, it can be seen that there is negligible difference in OCV and a 2–3 % change in internal impedance. Our assertion is that this variation is caused by drilling and the removal of material from the internal tab-weld that links the current collector to the aluminium can.

2.4. Reference performance test (RPT)

A reference performance test (RPT) was used to verify the electrochemical performance of the instrumented cells. During the RPT, cell discharge capacity and DC internal resistance (DCIR) were measured to identify the occurrence of any detrimental effect of the instrumentation process on cell performance. An RPT was undertaken at three stages of the instrumentation process: (i) on the pristine cell before any modification, (ii) after the cells were engineered to accept the sensor and finally (iii) after sensor insertion and re-sealing. This characterisation procedure comprised a constant-current – constant voltage (CC - CV) measure of energy capacity at current magnitudes 1C and C/10. During each test the transition to constant voltage occurred at 4.2 V, with the charge continuing until the value of current reduced below C/20. The power capability of the cells was evaluated through sequence of pulse discharges, in which a current magnitude of 2C and C/2 was applied for a duration of 10 s at SOC levels of 100 %, 80 %, 50 % and 20 %. In Fig. 7, the RPT characterisation procedure is illustrated, showing cell voltage and applied current.

All experiments were conducted within climate chamber set to 25 °C. Cells were placed in the chamber for 2 h before characterisation to allow them to reach thermal equilibrium. RPT characterisation was performed using a Bio Logic VSP-300 Potentiostat. Cell parameters during the RPT were logged at a sample frequency of 1 kHz during pulse discharge tests and 1 Hz for other stages (i.e. rest or lower charge and discharge stages).

The divergence between internal (core) and surface temperature was investigated during RPT characterisation. In order to accurately measure surface temperature, a commercial thermocouple (K-type, Pico Technology, UK) was attached to the centre location of the aluminium can. Ensuring the internal and external sensors were radially aligned allows for a robust comparison of core vs surface temperature during electrical loading. These surface thermocouples offered 1.5 °C accuracy, and a 0.7 s response time [30]. All temperature data were gathered using a data logger (TC-08, Pico Technology, UK) and analysed using MATLAB 2021b analytical software.

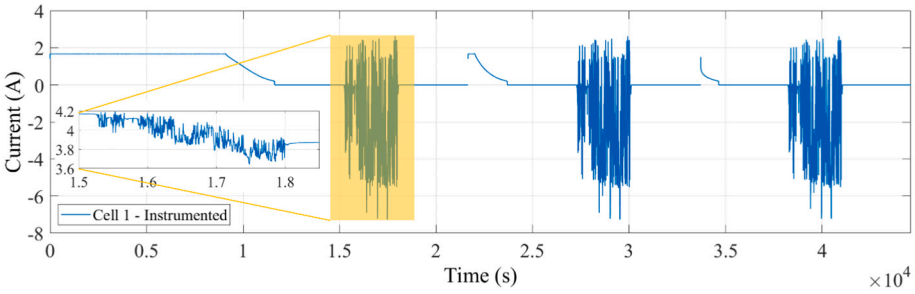

Fig. 8. Example current profile applied to the instrumented cells during load-profile cycling.

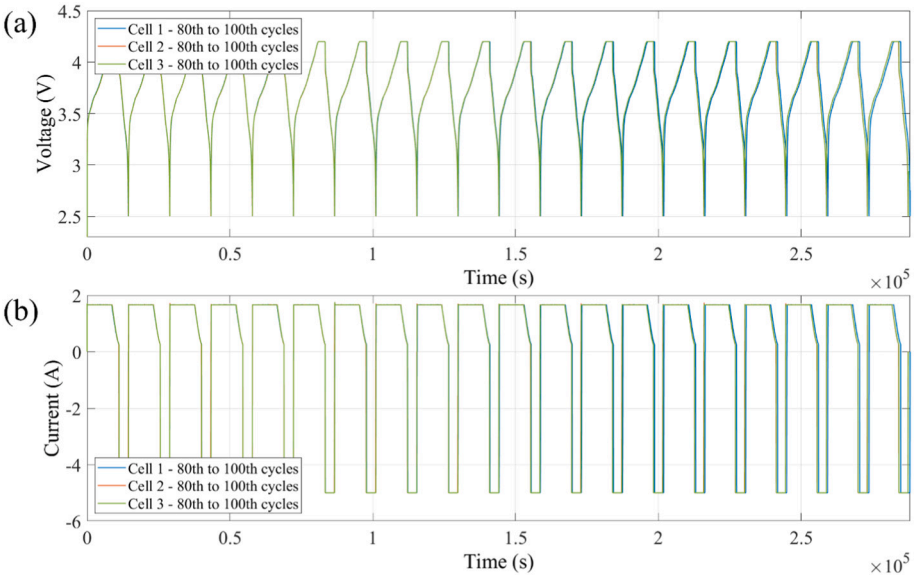

Fig. 9. (a) Cell voltage during ageing cycles (80–100) with instrumented cell 1; (b) Applied current.

2.5. Load-profile cycling

The operational stability of the embedded thermocouples and instrumented cells was investigated after the sensors had remained inside the cell cavity for a period of two months (stored at 25 °C). To quantify if there is an adverse effect on sensor and cell operation (e.g. due to corrosion of the sensor within the electrolyte or excessive calendar ageing) a dynamic load profile was applied to each cell. The starting SOC was varied from 100 %, 80 % and 50 %. The load profile was derived from research published by Niri et al. [31]. This contains a current profile of a real vehicle being driven in an urban environment for 45 min. The current measurements were extracted from the profile and scaled to suit the maximum charge and discharge current of the LG-M50 cell (defined by the manufacturer). The modified load profile consisted of a transient current up to 2.5 A charge and 7.5 A discharge. This rapid current variation (1 s steps) was selected to demonstrate the sensors stability during a fluctuating profile, and to demonstrate their potential for deployment in a real-world application. The applied load profile at each SOC threshold is shown in Fig. 8. The load-profile was applied using a Bio Logic VSP-300 Potentiostat with cells located in an environmental chamber set to 25 °C.

2.6. Degradation assessment

The potential for the instrumented cells to age faster than conventional cells was investigated. The reduction in retained energy capacity and change in internal resistance of the instrumented cells was quantified. All cells were repeatedly electrically loaded for 100 cycles. At intervals of 20 cycles the RPT process (Section 3.4) was repeated to define the cell's retained energy and impedance. To facilitate a comparison, three reference cells were also cycled under the same conditions.

During cell cycling, charge and discharge rates of C/3 and 1C were employed respectively. All cells were charged to the upper voltage limits of 4.2 V using a CC-CV procedure. Termination of the CV stage occurred when the applied current reduces below C/20. During discharge, a CC current was applied to the cells until a lower cut-off voltage of 2.5 V was reached. A rest period of 1 min was allowed before commencing the next charge-discharge cycle. A subset of the ageing procedure is illustrated in Fig. 9, showing both the applied current and terminal voltage. The ageing study was performed on a Digatron cycler MCT, while all RPT characterisation tests were performed using a Bio Logic VSP-300. Electrical loading and characterisation were performed with the cells located in a thermal chamber with the ambient temperature controlled to 25 °C.

3. Results and discussion

3.1. Understanding the instrumented cell performance based on discharge capacity

Fig. 10 summarises the effect of cell instrumentation on cell performance, in terms of discharge capacity measured from each RPT test during instrumentation. The median discharge energy capacity of three instrumented cells was found to be 4.83 Ah, which was identical to that found for the pristine cells. However, a small capacity rise of approximately 0.5 Ah was observed after cell modification. The median capacity

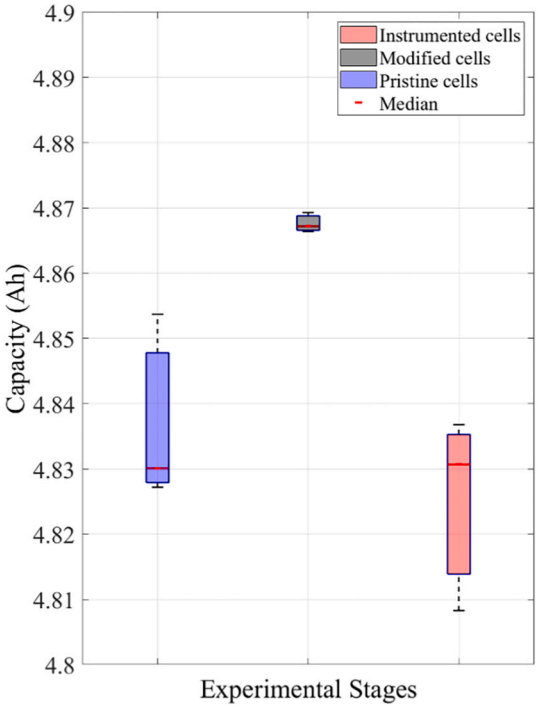

Fig. 10. Energy capacity of three LG-M50 cells for pristine, modified, and instrumented cell conditions.

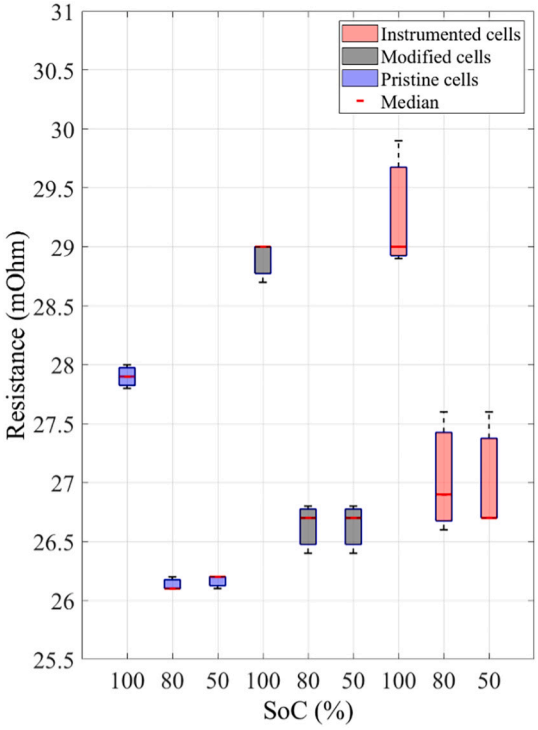

Fig. 11. DC internal resistance of three LG-M50 cells at specified SOC levels (100 %, 80 % and 50 %) for pristine, modified, and instrumented cell conditions.

of the modified cells was found to be 4.87 Ah. Further investigation is needed to determine the reason for this capacity rise and to identify the repeatability of this result.

The consistency of the value of discharge capacity between pristine and instrumented cells indicates that the instrumentation process has not been impacted by electrolyte loss and material damage due to cell modification, sensor insertion and sealing [10,32].

3.2. Understanding the instrumented cell based on DC internal resistance (DCIR)

Fig. 11 summarises the variations in measured DCIR obtained from the RPTs during instrumentation. The effect of cell modification (e.g. forming a tapped hole in the current collector), sensor insertion and sealing processes were analysed. The DCIR of all cells was obtained from a 2C pulse discharge test. For the pristine cells, the median DCIR of the three cells was found to be 27.9 mΩ at 100 % SOC, 26.1 mΩ at 80 % SOC and 26.2 mΩ at 50 % SOC. A small increase was found in the DCIR values after cell modification, this was calculated to be 1.1 mΩ at 100 % SOC, 0.6 mΩ at 80 % SOC and 0.5 mΩ at 50 % SOC. The reason for this increase is assumed to be caused by forming a hole in the current collector. After cell modification, a 4.91 mm^2 decrease in the surface area of the current collector was observed, as shown in Fig. 4(b). This corresponds with an observed rise in DCIR. When comparing the DCIR values of the modified cells against the instrumented cells, it was verified that the median DCIR was not affected by sensor insertion, where the same DCIR values were recorded.

3.3. Difference between internal and surface temperature

Fig. 12 highlights the temperature difference between the measured core and surface during RPT assessment. At the end of cell discharge (1C), the peak internal temperatures were observed to be 37 °C, 37.5 °C and 37.3 °C for cells 1, 2 and 3, respectively. The peak surface temperatures were recorded respectively as 33.7 °C, 34.6 °C and 34 °C for the same cells. Our results indicate that the internal temperature is approximately 4 °C higher than that measured on the cell's surface. This significant variation demonstrates the importance of core temperature measurement, even when the cells are cycled in a controlled manner, at a modest rate, within the manufacturer's recommendations. Deviation between internal and surface temperature is known to increase further during high current rate charging and discharging and during the onset of cell failure such as thermal runaway. Preliminary studies show a 100 °C temperature differential between core and surface during thermal runaway [33].

A comparison between Fig. 12(a) and (b) shows that the thermocouple on the surface of cell 2 did not detect the small temperature changes which could be observed from the associated sensor located within the cell. The surface sensor on cell 1 was able to measure similar fluctuations, demonstrating the inconsistency of surface measurements, and the caution required when examining cell performance using a limited dataset. The surface temperature of cell 2 was approximately 25 °C during pulse discharge tests (variation of <0.5 °C), whereas that of cell 1 reached 26.5 °C during higher current pulse discharge tests. Similar thermal characteristics were also observed during cell discharging (highlighted in the plot via a yellow rectangle). Surface temperature of cell 2 was measured as 24.8 °C, whereas at the same period during the cycle, 26.7 °C was recorded for cell 1. We propose this inconsistency could be caused by the difficulty in locating external sensors radially and axially in the identical location between cells. In this work, we positioned the cells axially precisely in the centre of the cell (35 mm from each terminal). Radially we positioned each sensor on the top surface of each cylindrical cell. The location of the current collectors (the thin internal tabs linking the jelly roll to each terminal) is not observably externally. In the cylindrical cells the negative current collector is positioned along the outside of the jelly roll, internally next to the can – visible in the top of Fig. 6(a). Without a CT scan image for each cell with a visible external reference, it is not possible to verify if external sensors are placed radially on-top of the current collector. The radial alignment and proximity of the sensor to the current collector (i.e., location in the y axis) could cause inconsistency in surface

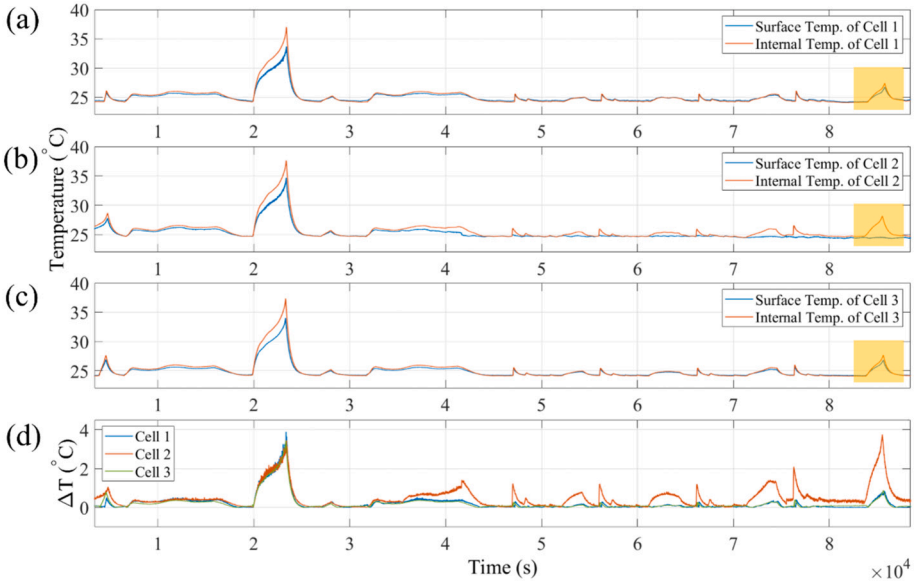

Fig. 12. (a) to (c) Internal and external temperatures measured during the RPT for instrumented cell 1, 2 and 3; (d) Delta temperature, which shows the difference between internal and external temperatures.

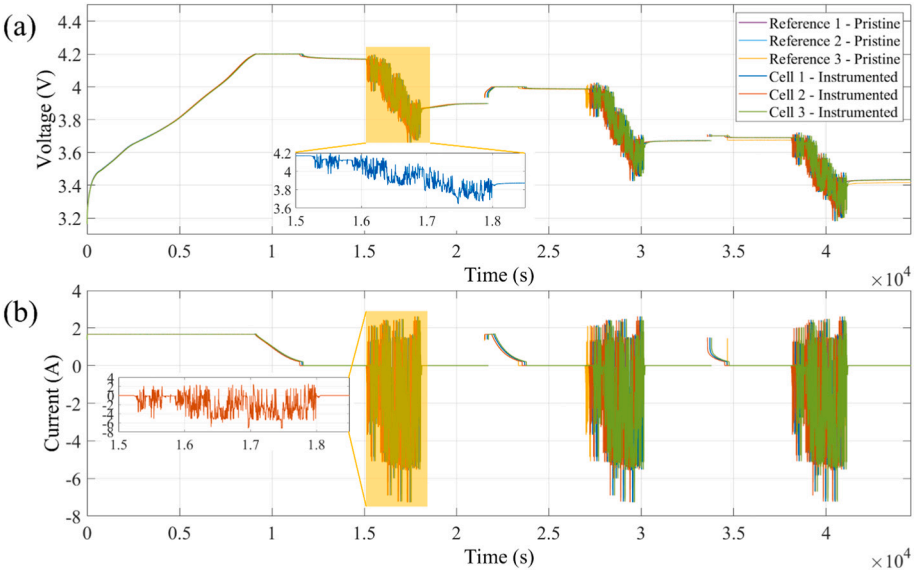

Fig. 13. (a) Cell voltage recorded during the load-profile cycling with reference and instrumented cells; (b) Current profile applied to the cells during the load-profile cycling.

measurements [6]. These results reinforce those reported previously in the literature, where surface temperature data is found to poorly correspond to internal readings, and at worst can provide inaccurate data towards cell health estimation [4,6,10]. Amietszajew et al. observed that the internal temperature exceeded the surface by 6 °C during a 1C discharge [10]. Since core temperature is noticeably higher than surface temperature, Fleming et al. also concludes that assumptions made about the battery according to surface temperature might be a misleading indicator when employed to predict battery failure and set safety limits [18].

3.4. Stability of instrumented cell operation

Fig. 13(a) shows the voltage response of all cells when the dynamic load-profile in Fig. 13(b) is applied. In preliminary testing, this profile was tested with pristine cells. Negligible variation in cell voltage was observed between these preliminary tests and the instrumented cell voltage presented below. No adverse effects (e.g. sudden decrease or increase in voltage or temperature) were observed when the profile was repeated at 100 %, 80 % and 50 % SOC levels. This underlines that the storage of the instrumented cells at 25 °C for 2 months after instrumentation did not negatively impact their operation.

Fig. 14 shows the internal and surface temperature variations during electrical cycling. As highlighted, when the current is less than C/2, there was no significant temperature difference between internal and surface measurements for all SOC% thresholds. For all three instrumented cells, variations in temperature was observed to be <0.5 °C during the first 800 s of cycling. However, the changes in temperature for all cells increased when subject to higher C rates. The observed temperature rise was noted to vary with SOC, where lower SOCs demonstrated a greater rise of nearly 1.5 °C at 50 % SOC.

Our results show that the performance of the embedded research

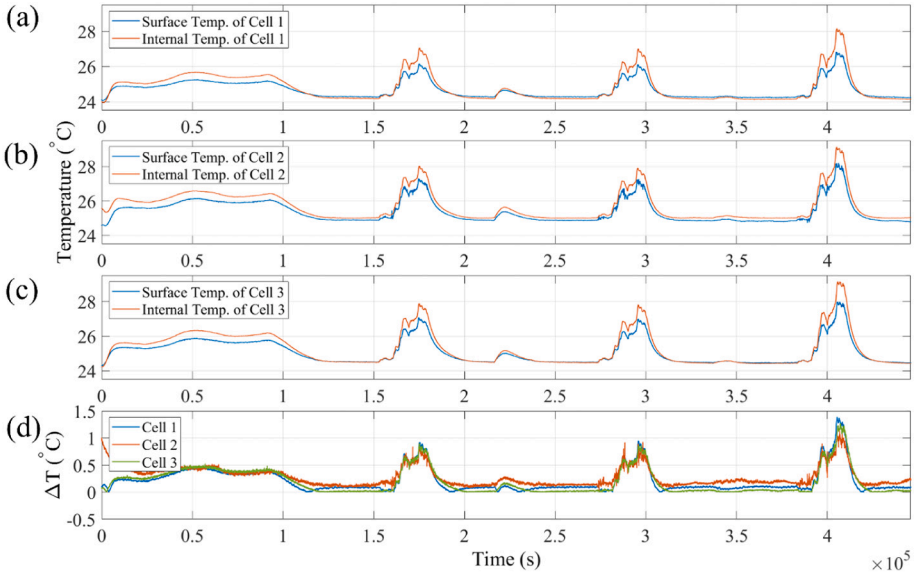

Fig. 14. (a) to (c) Internal and external temperatures measured during the cycling experiment for instrumented cell 1, 2 and 3, respectively; (d) Delta temperature, which shows the difference between internal and external temperatures during the cycling, for all three instrumented cells.

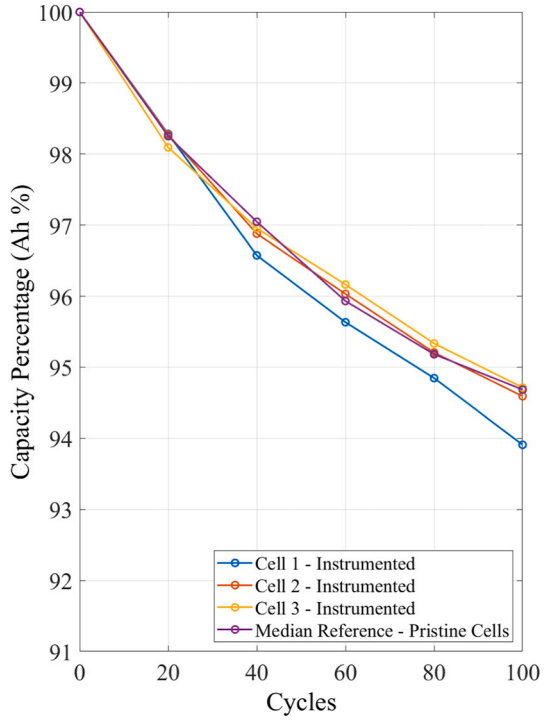

Fig. 15. Comparison of discharge capacity for reference and instrumented cells.

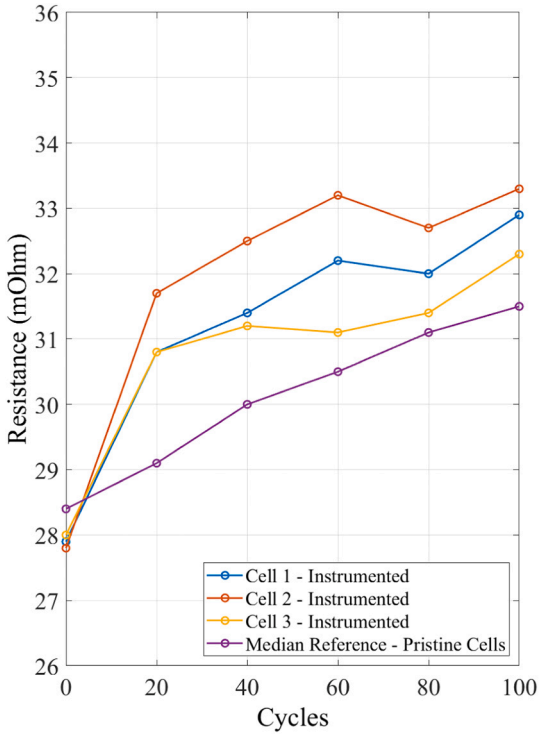

Fig. 16. DC internal resistance at 100 % SOC during ageing cycling for reference and instrumented cells.

thermocouples is not degraded by the harsh chemical environment within the cell. Furthermore, the materials used in sensor construction and the instrumentation methods employed do not adversely affect cell operation.

3.5. Degradation characteristics of instrumented cells

The relative reduction in energy capacity of both the instrumented and reference cells is shown in Fig. 15. For all reference and instrumented cells, the discharge capacity of the cells at the pristine stage was considered as an initial cell capacity (e.g. 100 %). This value was calculated as 4.83 Ah for both reference and instrumented cells. As highlighted by Fig. 15 the median capacity fade of pristine cells was found to be 5.2 % after 100 cycles. Comparing the capacity fade between the reference and instrumented cells, instrumented cell 2 and cell 3 there was no significant difference in retained capacity. However, the capacity fade for instrumented cell 1 was found to be slightly higher, at 6 % after 100 ageing cycles.

The DCIR results of all instrumented cells after cycling are shown in Fig. 16. For reference cells, the median DCIR was found to be 31.5 mΩ after 100 cycles. A 3 mΩ increase was observed compared to

Table 4
Internal and surface temperatures after 20 and 100 cycles.

Cell No	After 20 cycles			After 100 cycles		
	Internal temperature (~°C)	Surface temperature (~°C)	ΔT (~°C)	Internal temperature (~°C)	Surface temperature (~°C)	ΔT (~°C)
Cell 1	36.7	34.1	3.5	38.8	34.9	3.9
Cell 2	38	34.8	3.2	38.7	35.1	3.6
Cell 3	36.4	32.9	3.5	37	32	5

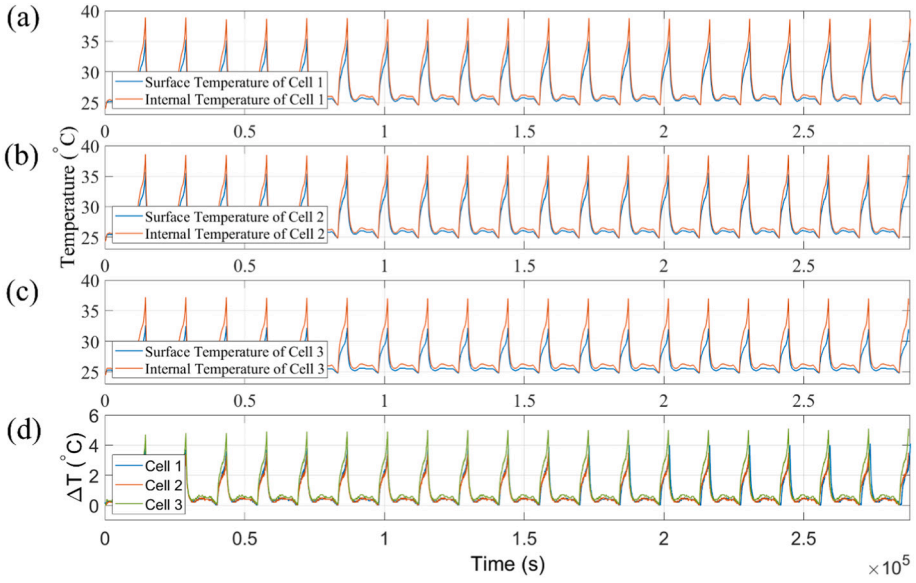

Fig. 17. (a) to (c) Internal and external temperatures measured during cycling for instrumented cell 1, 2 and 3; (d) Variation in temperature (internal vs external) during ageing.

measurements taken prior to cycle ageing. For the instrumented cells, the DCIR increased to 33 mΩ, 33.2 mΩ and 32.2 mΩ for instrumented cell 1, 2 and cell 3, respectively.

In our short-term study, the capacity fade and DCIR during 100 cycles demonstrated that there is no significant difference between instrumented cells and reference cells. We propose this indicates that our instrumentation method does not have a noticeable adverse effect on cell degradation. These initial short-term results successfully illustrate the success of our novel instrumentation method - we propose this work will be continued, to verify the degradation of our instrumented cells is comparable to non-modified cells over a longer-term (e.g. 600 cycles).

A comparison between peak temperatures (surface vs internal) during RPT testing are compared in Table 4. On average, the temperature difference between cell internal and surface was found to be 3.4 °C after 20 cycles. However, this value increases to 4.2 °C after 100 cycles. These results are shown graphically in Fig. 17. This result reinforces the view that the difference between internal and external battery states will often diverge as the battery ages and its SOH reduces [34,35].

Fig. 17 illustrates the temperature variation during the last 20 cycle of ageing.

4. Further work

Further research is required to extend this research into instrumented cells to cover the advanced characterisation of cells and the possible deployment of instrumented cells within future battery systems for transport and intelligent stationary storage applications.

Initial results, highlighted a possible dependency between the rise in internal temperature and battery SOC. Further research is required to fully understand this causality across the entire SOC region taking into account changes in the electrochemical performance of the battery at different SOC states. The results presented here are representative of our entire dataset (including preliminary work, comprising in the order of tens of cells tested). To better validate the methodology employed and in particular, to support the findings that cell performance and life are unaffected, a larger number of cells will be augmented with additional instrumentation for experimentation. The authors have confidence in the validity of the experimental results presented, although note due to the relatively small sample size of cells evaluated here, in our future work we aim to continue our instrumented cell development, consisting of low-volume production runs, to strengthen our statistical evidence and rigorous comparison to pristine cells.

The research presented here has demonstrated the measurement of in-cell temperature within a cylindrical cell. It is likely that this methodology will be transferable to other cell formats providing geometric factors, e.g., solid mandrel and additional safety features, e.g., pressure release features do not impede entry into the cell. In addition, the test fixtures and sensor-adaptors would require modification based on the revised geometry of the cell and its internal structure identified through engineering documentation and CT imaging. Further research is required to assess the transferability of the methodology to other cell formats such larger prismatic and multi-layered pouch cells.

The instrumented cells developed in this research have been employed to quantify cell operation during normal use. Further research is required to assess the suitability of the sensors and cell engineering techniques when quantifying cell performance under extreme use cases, such as overcharge, undercharge, higher ambient temperatures or mechanical excitation. The ability to reproducibly and repeatably measure internal battery states under conditions potentially leading to thermal runaway are particularly pertinent given that breakdown in the structure of the battery is known to further extend the difference between internal to surface measurements. The integrity of sensors in contact

with harsh environment of thermal runaway needs to be appraised, e.g., resolution and accuracy in elevated temperature and pressure measurements. Further, when undertaking such advanced characterisation, the use of additional sensors to measure internal pressure and electrode strain may yield greater insights into cell performance and life. Further work is required to understand the transferability of the techniques to other sensor types, including the ability to insert multi-sensor arrays within a single cell.

In addition to the use of instrumented cells for laboratory characterisation, such cells may be deployed within battery systems to extend current battery management operation and to estimate key battery states in real-time. Further research is required to optimise the inclusion of instrumented cells within a battery system, including their selective use at certain locations in the battery pack to allow the control system to quantify variations in temperature, pressure and charge that may occur during operation.

5. Conclusion

A systematic and rigorous methodology for cell modification, instrumentation and verification has been presented. Experimental results, encompassing operational performance and the assessment of cell degradation highlight that the performance and life of instrumented cells are not adversely affected. In this research, internal temperature monitoring in operando was achieved by embedding temperature sensors within the interior of three cells, where damage to the cell structure was minimised during sensor insertion and sealing. Our study demonstrates the importance of internal temperature monitoring during cell operation by comparing internal and surface measurements. We found that the internal temperature is consistently and notably higher than the surface temperature during our standard RPT and load-profile cycles. The difference between internal and surface temperatures was observed to be typically 4 °C during normal operation. CT images of the cells at key stages of the instrumentation process highlight the minimal impact to the physical structure of the cell. Any variations in performance and life were quantified through comparative studies with pristine cells, where no significant effect on electrochemical performance was observed. We used a comprehensive verification method to measure cell discharge capacity and DC internal resistance. This process was performed both before and after instrumentation. Measurement data demonstrates that there is a negligible reduction in energy capacity and a marginal increase in internal resistance. Further the degradation rate of our instrumented cells was comparable to conventional cells when subject to both calendar and cyclic ageing tests.

CRediT authorship contribution statement

B.G., T.A.V. and J.E.H.S. performed experiments and B.G. analysed the data. J.E.H.S. and J.M. research definition, supervision and manuscript editing. B.G. and T.A.V publication writing, with contributions from all authors.

Declaration of competing interest

The authors declare that they have no known competing financial interests or personal relationships that could have appeared to influence the work reported in this paper.

Acknowledgements

This work was supported by the WMG High Value Manufacturing Catapult, Part-funded by Innovate UK.

Data availability

The data generated and analysed during the current study are not publicly available for legal/ethical reasons but are available from the corresponding author on reasonable request.

References

[1] The Internal Council on Clean Transportation (ICCT), Vision 2050: A strategy to decarbonize the global transport sector by mid-century - International Council on Clean Transportation [Online]. Available: https://theicct.org/publication/vision-2050-a-strategy-to-decarbonize-the-global-transport-sector-by-mid-century/ [Accessed: 17-Mar-2022].

[2] E. Hosseinzadeh, et al., Quantifying cell-to-cell variations of a parallel battery module for different pack configurations [Online]. Available: http://wrap.warwick.ac.uk/142117, 2020 [Accessed: 17-Mar-2022].

[3] X. Liu W. Ai M. N. Marlow Y. Patel B. Wu "The effect of cell-to-cell variations and thermal gradients on the performance and degradation of lithium-ion battery packs".

[4] G. Zhang, L. Cao, S. Ge, C.-Y. Wang, C.E. Shaffer, C.D. Rahn, In situ measurement of radial temperature distributions in cylindrical Li-ion cells, J. Electrochem. Soc. 161 (10) (Jul. 2014) A1499–A1507, https://doi.org/10.1149/2.0051410jes [Online]. Available: https://iopscience.iop.org/article/10.1149/2.0051410jes. [Accessed: 15-Jun-2021].

[5] J. Zhang, L. Zhang, F. Sun, Z. Wang, An overview on thermal safety issues of lithium-ion batteries for electric vehicle application, IEEE Access 6 (May 2018) 23848–23863, https://doi.org/10.1109/ACCESS.2018.2824838.

[6] Y. Yu, et al., Distributed thermal monitoring of lithium ion batteries with optical fibre sensors, J. Energy Storage 39 (Jul. 2021), 102560, https://doi.org/10.1016/j.est.2021.102560.

[7] M.S. Wahl, L. Spitthoff, H.I. Muri, A. Jinasena, O.S. Burheim, J.J. Lamb, The importance of optical fibres for internal temperature sensing in lithium-ion batteries during operation, Energies 14 (12) (Jun. 2021) 3617, https://doi.org/10.3390/EN14123617, 2021, Vol. 14, Page 3617.

[8] E. Vergori, Y. Yu, Monitoring of li-ion cells with distributed fibre optic sensors, Procedia Struct. Integr. 24 (2019) 233–239, https://doi.org/10.1016/j.prostr.2020.02.020.

[9] E. McTurk, T. Amietszajew, J. Fleming, R. Bhagat, Thermo-electrochemical instrumentation of cylindrical Li-ion cells, J. Power Sources 379 (Mar. 2018) 309–316, https://doi.org/10.1016/j.jpowsour.2018.01.060.

[10] T. Amietszajew, E. McTurk, J. Fleming, R. Bhagat, Understanding the limits of rapid charging using instrumented commercial 18650 high-energy Li-ion cells, Electrochim. Acta 263 (Feb. 2018) 346–352, https://doi.org/10.1016/J.ELECTACTA.2018.01.076.

[11] J. Fleming, T. Amietszajew, E. McTurk, D. Greenwood, R. Bhagat, Development and evaluation of in-situ instrumentation for cylindrical Li-ion cells using fibre optic sensors, HardwareX 3 (2018) 100–109, https://doi.org/10.1016/j.ohx.2018.04.001.

[12] M. Fleckenstein, O. Bohlen, M.A. Roscher, B. Bäker, Current density and state of charge inhomogeneities in Li-ion battery cells with LiFePO4 as cathode material due to temperature gradients, J. Power Sources 196 (10) (May 2011) 4769–4778, https://doi.org/10.1016/J.JPOWSOUR.2011.01.043.

[13] R. Srinivasan, P.A. Demirev, B.G. Carkhuff, Rapid monitoring of impedance phase shifts in lithium-ion batteries for hazard prevention, J. Power Sources 405 (Nov. 2018) 30–36, https://doi.org/10.1016/j.jpowsour.2018.10.014.

[14] P.V. Chombo, Y. Laoonual, A review of safety strategies of a Li-ion battery, J. Power Sources 478 (Dec. 2020), 228649, https://doi.org/10.1016/J.JPOWSOUR.2020.228649.

[15] R.R. Richardson, S. Zhao, D.A. Howey, On-board monitoring of 2-D spatially-resolved temperatures in cylindrical lithium-ion batteries: part II. State estimation via impedance-based temperature sensing, J. Power Sources 327 (Sep. 2016) 726–735, https://doi.org/10.1016/j.jpowsour.2016.06.104.

[16] C. Xu, et al., Internal temperature detection of thermal runaway in lithium-ion cells tested by extended-volume accelerating rate calorimetry, J. Energy Storage 31 (Oct. 2020), 101670, https://doi.org/10.1016/j.est.2020.101670.

[17] T.A. Vincent, B. Gulsoy, J.E.H. Sansom, J. Marco, Development of an in-vehicle power line communication network with in-situ instrumented smart cells, Transp. Eng. (Nov. 2021) 100098, https://doi.org/10.1016/J.TRENG.2021.100098.

[18] J. Fleming, T. Amietszajew, J. Charmet, A.J. Roberts, D. Greenwood, R. Bhagat, The design and impact of in-situ and operando thermal sensing for smart energy storage, J. Energy Storage 22 (Apr. 2019) 36–43, https://doi.org/10.1016/j.est.2019.01.026.

[19] L. Yang, et al., Internal field study of 21700 battery based on long-life embedded wireless temperature sensor, Acta Mech. Sin. 1 (Jun. 2021) 1–7, https://doi.org/10.1007/S10409-021-01103-0, 2021.

[20] S. Novais, et al., Internal and external temperature monitoring of a Li-ion battery with fiber Bragg grating sensors, Sensors 16 (9) (Aug. 2016) 1394, https://doi.org/10.3390/s16091394.

[21] A. Jinasena, et al., Online internal temperature sensors in lithium-ion batteries: state-of-the-art and future trends, Front. Chem. Eng. (Feb. 2022) 6, https://doi.org/10.3389/FCENG.2022.804704.

[22] C. Alippi, C. Alippi, Intelligent mechanisms in embedded systems, in: Intelligence for Embedded Systems, Springer International Publishing, Zurich, 2014, pp. 159–210.

[23] T. Grandjean, A. Barai, E. Hosseinzadeh, Y. Guo, A. McGordon, J. Marco, Large format lithium ion pouch cell full thermal characterisation for improved electric vehicle thermal management, J. Power Sources 359 (2017) 215–225, https://doi.org/10.1016/j.jpowsour.2017.05.016.

[24] T. Waldmann, et al., Electrochemical, post-mortem, and ARC analysis of Li-ion cell safety in second-life applications, J. Electrochem. Soc. 164 (13) (2017) A3154–A3162, https://doi.org/10.1149/2.0961713jes.
[25] J.R. Belt, D.M. Bernardi, V. Utgikar, Development and use of a lithium-metal reference electrode in aging studies of lithium-ion batteries, J. Electrochem. Soc. 161 (6) (May 2014) A1116–A1126, https://doi.org/10.1149/2.062406jes [Online]. Available: https://iopscience.iop.org/article/10.1149/2.062406jes. [Accessed: 15-Jun-2021].
[26] G. Liu, L. Zhang, Research on the thermal characteristics of an 18650 lithium-ion battery based on an electrochemical–thermal flow coupling model, 2021, Vol. 12, Page 250, World Electr. Veh. J. 12 (4) (Nov. 2021) 250, https://doi.org/10.3390/WEVJ12040250 [Online]. Available: https://www.mdpi.com/2032-6653/12/4/250/htm. [Accessed: 17-Mar-2022].
[27] R.S.W.Kim Young-Soo, "<article-title>PRODUCT SPECIFICATION Rechargeable Lithium Ion Battery Model: INR21700 M50 18.20Wh</article-title>," LG Chem [Online]. Available: https://www.dnkpower.com/wp-content/uploads/2019/02/LG-INR21700-M50-Datasheet.pdf [Accessed: 07-Feb-2022].
[28] H. Popp, et al., Ante-mortem analysis, electrical, thermal, and ageing testing of state-of-the-art cylindrical lithium-ion cells, Elektrotechnik und Informationstechnik 137 (4–5) (Aug. 2020) 169–176, https://doi.org/10.1007/S00502-020-00814-9/FIGURES/6 [Online]. Available: https://link.springer.com/article/10.1007/s00502-020-00814-9. [Accessed: 07-Feb-2022].
[29] C.-H. Chen, F.Brosa Planella, K. O'Regan, D. Gastol, W.D. Widanage, E. Kendrick, Development of experimental techniques for parameterization of multi-scale lithium-ion battery models, J. Electrochem. Soc. 167 (8) (May 2020) 080534, https://doi.org/10.1149/1945-7111/ab9050 [Online]. Available: https://iopscience.iop.org/article/10.1149/1945-7111/ab9050. [Accessed: 15-Jun-2021].
[30] RS PRO Type K Thermocouple 5m Length, 1/0.2mm Diameter → +260°C | RS Components [Online]. Available: https://uk.rs-online.com/web/p/thermocouples/1236306?cjevent=eab1f8b713f58c3dd248f3d5b903c327d7c00cda0cd9b89f6&cm_mmc=UK-CJAFF-_-Genie+Shopping+CSS-_-RS++RS+Components+UK [Accessed: 08-Feb-2022].
[31] M.F. Niri, T.M.N. Bui, T.Q. Dinh, E. Hosseinzadeh, T.F. Yu, J. Marco, Remaining energy estimation for lithium-ion batteries via Gaussian mixture and Markov models for future load prediction, J. Energy Storage 28 (Apr. 2020), 101271, https://doi.org/10.1016/j.est.2020.101271.
[32] L. Willenberg, et al., The development of jelly roll deformation in 18650 lithium-ion batteries at low state of charge, J. Electrochem. Soc. 167 (12) (Aug. 2020), 120502, https://doi.org/10.1149/1945-7111/ABA96D [Online]. Available: https://iopscience.iop.org/article/10.1149/1945-7111/aba96d. [Accessed: 21-Oct-2021].
[33] M. Parhizi, M.B. Ahmed, A. Jain, Determination of the core temperature of a Li-ion cell during thermal runaway, J. Power Sources 370 (Dec. 2017) 27–35, https://doi.org/10.1016/J.JPOWSOUR.2017.09.086.
[34] X. Lin, et al., Online parameterization of lumped thermal dynamics in cylindrical lithium ion batteries for core temperature estimation and health monitoring, IEEE Trans. Control Syst. Technol. 21 (5) (Sep. 2013) 1745–1755, https://doi.org/10.1109/TCST.2012.2217143.
[35] J. Tian, R. Xiong, W. Shen, State-of-health estimation based on differential temperature for lithium ion batteries, IEEE Trans. Power Electron. 35 (10) (Oct. 2020) 10363–10373, https://doi.org/10.1109/TPEL.2020.2978493.